


RESEARCH PAPER

A two-state model for the kinetics of competitive radioligand binding

Correspondence Adriaan P IJzerman, Gorlaeus Lab/LACDR, Department of Medicinal Chemistry, Leiden University, Einsteinweg 55, 2333 CC Leiden, The Netherlands. E-mail: ijzerman@lacdr.leidenuniv.nl

Received 24 May 2017; **Revised** 11 December 2017; **Accepted** 19 February 2018

Dong Guo^{1,2} , Lambertus A Peletier³, Lloyd Bridge^{4,6}, Wesley Keur², Henk de Vries², Annelien Zweemer⁵, Laura H Heitman² and Adriaan P IJzerman²

¹Jiangsu Key Laboratory of New Drug Research and Clinical Pharmacy, Xuzhou Medical University, Xuzhou, Jiangsu, China, ²Division of Medicinal Chemistry, Leiden Academic Centre for Drug Research (LACDR), Leiden University, Leiden, The Netherlands, ³Mathematical Institute, Leiden University, Leiden, The Netherlands, ⁴Department of Mathematics, Swansea University, Swansea, UK, ⁵Department of Biological Engineering, Massachusetts Institute of Technology (MIT), Cambridge, MA, USA, and ⁶Department of Engineering Design and Mathematics, University of the West of England, Bristol, UK

BACKGROUND AND PURPOSE

Ligand–receptor binding kinetics is receiving increasing attention in the drug research community. The Motulsky and Mahan model, a one-state model, offers a method for measuring the binding kinetics of an unlabelled ligand, with the assumption that the labelled ligand has no preference while binding to distinct states or conformations of a drug target. As such, the one-state model is not applicable if the radioligand displays biphasic binding kinetics to the receptor.

EXPERIMENTAL APPROACH

We extended the Motulsky and Mahan model to a two-state model, in which the kinetics of the unlabelled competitor binding to different receptor states (R_1 and R_2) can be measured. With this extended model, we determined the binding kinetics of unlabelled *N*-5'-ethylcarboxamidoadenosine (NECA), a representative agonist for the adenosine A_1 receptor. Subsequently, an application of the model was exemplified by measuring the binding kinetics of other A_1 receptor ligands. In addition, limitations of the model were investigated as well.

KEY RESULTS

The kinetic rate constants of unlabelled NECA were comparable with the results of kinetic radioligand binding assays in which [³H]-NECA was used. The model was further validated by good correlation between simulated results and the experimental data.

CONCLUSION

The two-state model is sufficient to analyse the binding kinetics of an unlabelled ligand, when a radioligand shows biphasic association characteristics. We expect this two-state model to have general applicability for other targets as well.

Abbreviations

CHAPS, 3-[(3-cholamidopropyl)dimethylammonio]-1-propanesulfonate; CPA, *N*⁶-cyclopentyladenosine; DPCPX, 1,3-dipropyl-8-cyclopentylxanthine; LUF5962, 8-cyclopentyl-2,6-diphenyl-9*H*-purine; NECA, *N*-5'-ethylcarboxamidoadenosine

Introduction

The kinetics of ligand–receptor binding constitute a topic of increasing concern in the early phase of the drug design and discovery process. The importance of this topic has recently been emphasized in several reviews (Swinney, 2009; Copeland, 2016; Guo *et al.*, 2017). These discussions led to an increased recognition of the importance of binding kinetics in the preclinical stages of drug discovery. In particular, the drug–target residence time ($1 \cdot k_{\text{off}}^{-1}$) represents an experimental description of the stability of the ligand–receptor binary complex, which is suggested as a better predictor than steady-state metrics, such as affinity values, in terms of the duration of a pharmacological effect and target selectivity (Copeland *et al.*, 2006; Guo *et al.*, 2014; Swinney *et al.*, 2015).

Experimental approaches for kinetic measurements are available, and new technologies are emerging (Hoffmann *et al.*, 2015). Among current experimental strategies, kinetic radioligand binding assays enable straightforward kinetic profiling of a labelled ligand on a given receptor. However, the process of labelling compromises its practicability in large-scale determinations. Alternative strategies enabling quantitative kinetic profiling of unlabelled ligands have been developed (Motulsky and Mahan, 1984; Malany *et al.*, 2009; Packeu *et al.*, 2010). One representative method is the so-called competition association assay based on the mathematical model developed by Motulsky and Mahan (1984). This model can be described by the following pair of reaction equations:



Briefly, an unlabelled ligand of interest (i.e. the competitor, B) is co-incubated with a well-characterized radioligand (A), both competitively binding to the receptor (R). The competitor may delay the time-dependent increase of radioligand binding or even produce a time-dependent decrease in radioligand binding after an initial ‘overshoot’ (Packeu *et al.*, 2010). These procedures allow an accurate estimation of a competitor’s dissociation rate, as demonstrated by several analyses using GPCRs (Dowling and Charlton, 2006; Guo *et al.*, 2012, 2013; Vilums *et al.*, 2013; Nederpelt *et al.*, 2016) as well as the **K_v11.1** ion channel (Yu *et al.*, 2015). The model is applied with the assumption that the labelled ligand has no preference while binding to distinct receptor states or conformations, hence representing a one-state model (R). However, it is known that a radioligand may display biphasic binding characteristics to the receptor. For instance, an agonist radioligand often has a strong preference for a given state of a GPCR over another, thus resulting in a biphasic association (Munshi *et al.*, 1985; van Veldhoven *et al.*, 2015). In this situation, the one-state model is no longer applicable for quantitative kinetic measurements.

In the present study, we have extended the Motulsky and Mahan model into a two-state receptor model (R₁ and R₂) that enables kinetic profiling of an unlabelled competitor using a radioligand that displays biphasic kinetic radioligand binding. The human adenosine A₁ receptor was used as a prototypical target. For model validation, the binding kinetics of an unlabelled adenosine receptor agonist, N-5'-ethylcarboxamidoadenosine (**NECA**), was measured and

analysed using the two-state receptor model and compared with the kinetic parameters obtained with the tritiated probe [³H]-**NECA** in a classical association and dissociation experiment. The model was further validated by comparing simulated results with the experimental data. Furthermore, the kinetics of another unlabelled agonist, N⁶-cyclopentyladenosine (**CPA**), was measured and analysed to demonstrate the applicability of this novel two-state model. Finally, the model was also used to study the binding kinetics of two antagonists, 1,3-dipropyl-8-cyclopentylxanthine (**DPCPX**) and 8-cyclopentyl-2,6-diphenyl-9H-purine (**LUF5962**).

Methods

Group sizes

Numbers (*n*) for all experiments are provided and refer to independent single measurements.

Randomization

Randomization was not applicable, hence not performed.

Blinding

Blinding of experiments is not applicable.

Cell culture and membrane preparation

Cell culture and membrane preparation were performed as reported previously (Guo *et al.*, 2013). CHO cells stably expressing the human **adenosine A₁ receptor** (CHOhA₁R cells) were grown in Ham’s F12 medium containing 10% (v/v) normal adult bovine serum, streptomycin (100 µg·mL⁻¹), penicillin (100 IU·mL⁻¹) and G418 (0.4 mg·mL⁻¹) at 37°C in 5% CO₂. Cells were subcultured twice weekly at a ratio of 1:20 on 10 cm diameter culture plates.

For membrane preparation, cells were subcultured 1:10 and then transferred to 15 cm plates. Cells grown to 80 to 90% confluency were detached from plates by scraping them into 5 mL PBS, collected and centrifuged at 700 × *g* for 5 min. Cell pellets derived from 30 plates were pooled and resuspended in 20 mL of ice-cold 50 mM Tris–HCl buffer (pH 7.4). An UltraTurrax (Heidolph Instruments, Schwabach, Germany) was used to homogenize the cell suspension. Membranes and the cytosolic fraction were separated by centrifugation at 100 000 × *g* in a Beckman Optima LE-80K ultracentrifuge (Beckman Coulter, Fullerton, CA) at 4°C for 20 min. The pellet was resuspended in 15 mL of the Tris–HCl buffer, and the homogenization and centrifugation step were repeated. Tris–HCl buffer (10 mL) was used to resuspend the pellet, and **adenosine deaminase** (0.8 IU·mL⁻¹) was added to break down endogenous adenosine. Membranes were stored in 250 µL aliquots at –80°C. Concentrations of the membrane protein were measured using the bicinchoninic acid assay method (Smith *et al.*, 1985).

Competition binding assays

Membrane aliquots containing 40 µg of protein were incubated in a total volume of 100 mL of assay buffer (50 mM Tris–HCl, pH 7.4, supplemented with 5 mM MgCl₂ and 0.1% w·v⁻¹ CHAPS) at 30°C for 3 h to ensure the equilibrium was reached. Radioligand displacement experiments were

performed using six concentrations of a competing ligand in the presence of ~18 nM [³H]-NECA. Non-specific binding was determined in the presence of 100 μM NECA and represented less than 10% of the total radioligand binding. All concentrations mentioned here and in following sections are final concentrations. Incubations were terminated by rapid vacuum filtration to separate the bound and free radioligand through Whatman GF/B filters (Whatman International, Maidstone, UK) with a Brandel harvester or using a PerkinElmer Filtermate harvester (Groningen, The Netherlands). Filters were washed 3 times with ice-cold wash buffer (50 mM Tris-HCl, 5 mM MgCl₂, pH 7.4). The filter-bound radioactivity was determined by scintillation spectrometry using a liquid scintillation counter (Tri-Carb 2900 TR, PerkinElmer) or a Microbeta Wallac Trilux scintillation counter (P-E 1450, Perkin Elmer).

Kinetic radioligand binding experiments

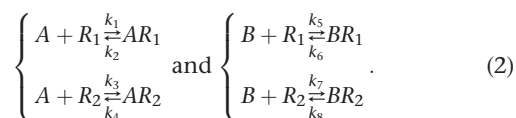
Association experiments were performed by incubating membrane aliquots containing 40 μg of protein in a total volume of 100 μL of assay buffer with ~18 nM [³H]-NECA at 30°C. The amount of radioligand bound to the receptor was measured at different time intervals during incubation for 3 h. Dissociation experiments were performed by preincubating CHO_{hA1R} cell membranes in a total volume of 100 μL of assay buffer with ~18 nM [³H]-NECA at 30°C for 2 h. Subsequently, the dissociation was initiated by addition of 10 μM DPCPX in 5 μL. The amount of radioligand still bound to the receptor was measured at different time intervals for a total duration of 7 h at 30°C to ensure that the radioligand was fully dissociated from the receptor. Non-specific binding was determined in the presence of 100 μM NECA and represented less than 10% of the total radioligand binding. Incubations were terminated, and samples were obtained as described under *Competition binding assays*.

Two-state competition association assays

The binding kinetics of unlabelled ligand were determined at 30°C using the two-state model as mentioned below. The experiment was initiated by adding membrane aliquots containing 40 μg of protein at different time points to a total volume of 100 μL assay buffer with ~18 nM [³H]-NECA in the absence or presence of a competing ligand at three concentrations (approximately 0.3×, 1× and 3× IC₅₀). Incubations were terminated, and samples were obtained as described under *Competition binding assays*.

The two-state model

Here, we consider kinetics for a two-state receptor system (R₁ and R₂) and a radioligand (A) in the presence of an unlabelled competitor (B). Both bind reversibly to the receptors with specific kinetic constants following the law of mass action. This yields the following generalization of the model:



Here, k₁ and k₃ (M⁻¹·min⁻¹) are the association rate constants of the radioligand A binding to the R₁ and R₂ states,

respectively, and k₂ and k₄ (min⁻¹) are the dissociation rate constants of A from the R₁ and R₂ states respectively. Similarly, k₅ (M⁻¹·min⁻¹) and k₆ (min⁻¹) are the association and dissociation rate constants of the competitor (B) at the R₁ state, and k₇ (M⁻¹·min⁻¹) and k₈ (min⁻¹) are the association and dissociation rate constants of B at the R₂ state.

In this analysis, we assume that (i) there is no exchange between the R₁ and R₂ states; (ii) only a small fraction (<10%) of the radioligand binds to the receptor. Therefore, the free concentration of the radioligand is approximately constant and equal to the concentration added. Thus, the binding reaction and the conservation of mass lead to the following system of ordinary differential equations (ODEs):

$$\begin{cases} \frac{dAR_1}{dt} = k_1A \cdot R_{1,\text{tot}} - k_{A,R_1}AR_1 - k_1A \cdot BR_1 \\ \frac{dAR_2}{dt} = k_3A \cdot R_{2,\text{tot}} - k_{A,R_2}AR_2 - k_3A \cdot BR_2 \\ \frac{dBR_1}{dt} = k_5B \cdot R_{1,\text{tot}} - k_5B \cdot AR_1 - k_{B,R_1}BR_1 \\ \frac{dBR_2}{dt} = k_7B \cdot R_{2,\text{tot}} - k_7B \cdot AR_2 - k_{B,R_2}BR_2 \end{cases}, \quad (3)$$

where

$$k_{A,R_1} = k_1A + k_2 \text{ and } k_{A,R_2} = k_3A + k_4; \quad (4)$$

$$k_{B,R_1} = k_5B + k_6 \text{ and } k_{B,R_2} = k_7B + k_8; \quad (5)$$

and

$$R_{1,\text{tot}} = R_1 + AR_1 + BR_1 \text{ and } R_{2,\text{tot}} = R_2 + AR_2 + BR_2. \quad (6)$$

The system (Equation 3) can be viewed as a pair of two smaller systems, one for the ligand-receptor complexes AR₁ and BR₁ and one for the ligand-receptor complexes AR₂ and BR₂. Because there is no exchange of R₁ into R₂ and *vice versa*, that is, R_{1,tot} and R_{2,tot} are constant in time, these two systems are independent, each one of them comparable with the system studied by Motulsky and Mahan (1984). The system has a unique steady state (AR_{1,ss}; AR_{2,ss}, BR_{1,ss}, BR_{2,ss}) where the radioligand complexes are given by

$$\begin{cases} AR_{1,ss} = k_1A \cdot R_{1,\text{tot}} \frac{k_6}{k_{A,R_1}k_{B,R_1} - k_1k_5AB} \\ AR_{2,ss} = k_3A \cdot R_{2,\text{tot}} \frac{k_8}{k_{A,R_2}k_{B,R_2} - k_3k_7AB} \end{cases} \quad (7)$$

By assumption and experimental set-up, A and B are taken to be constant, and therefore, the system (Equation 3) is linear and can be solved by standard methods. Each sub-system consists of two equations, and the corresponding (2 × 2) matrix of the coefficients of AR_i and BR_i has two eigenvalues, denoted by -λ_{F,i} and -λ_{S,i} where λ_{F,i} > λ_{S,i} > 0 for i = 1,2. For the binding to R₁, they are given by

$$\begin{cases} \lambda_{F,1} = \frac{1}{2} \left\{ (k_{A,R_1} + k_{B,R_1}) + \sqrt{(k_{A,R_1} - k_{B,R_1})^2 + 4k_1k_5AB} \right\} \\ \lambda_{S,1} = \frac{1}{2} \left\{ (k_{A,R_1} + k_{B,R_1}) - \sqrt{(k_{A,R_1} - k_{B,R_1})^2 + 4k_1k_5AB} \right\} \end{cases}, \quad (8)$$

and for the binding to R₂, they are given by

$$\begin{cases} \lambda_{F,2} = \frac{1}{2} \left\{ (k_{A,R_2} + k_{B,R_2}) + \sqrt{(k_{A,R_2} - k_{B,R_2})^2 + 4k_3k_7AB} \right\} \\ \lambda_{S,2} = \frac{1}{2} \left\{ (k_{A,R_2} + k_{B,R_2}) - \sqrt{(k_{A,R_2} - k_{B,R_2})^2 + 4k_3k_7AB} \right\} \end{cases} \quad (9)$$

For the temporal behaviour of the ligand–receptor complex AR_1 and AR_2 , we then find the expressions

$$\begin{cases} AR_1(t) = AR_{1,ss} - P_1 e^{-\lambda_{F,1}t} - Q_1 e^{-\lambda_{S,1}t} \\ AR_2(t) = AR_{2,ss} - P_2 e^{-\lambda_{F,2}t} - Q_1 e^{-\lambda_{S,2}t} \end{cases} \quad (10)$$

where P_i and Q_i are constants to be determined from the initial conditions. It is assumed that initially, no radioligand and no competitor are bound to either receptor state, that is,

$$AR_1(0) = 0, \quad AR_2(0) = 0, \quad BR_1(0) = 0, \quad BR_2(0) = 0. \quad (11)$$

Using this in the expression given in Equation 10 as well as the differential equations, we obtain for the constants P_i and Q_i :

$$\begin{cases} P_1 = \frac{k_1 A \cdot R_{1,tot} - \lambda_{S,1} AR_{1,ss}}{\lambda_{F,1} - \lambda_{S,1}} \text{ and } Q_1 = \frac{\lambda_{F,1} AR_{1,ss} - k_1 A \cdot R_{1,tot}}{\lambda_{F,1} - \lambda_{S,1}} \\ P_2 = \frac{k_3 A \cdot R_{2,tot} - \lambda_{S,2} AR_{2,ss}}{\lambda_{F,2} - \lambda_{S,2}} \text{ and } Q_2 = \frac{\lambda_{F,2} AR_{2,ss} - k_3 A \cdot R_{2,tot}}{\lambda_{F,2} - \lambda_{S,2}} \end{cases} \quad (12)$$

Clearly, the solution of the system (Equation 3) can be expressed as the sum of the solutions of two sub-systems:

$$\begin{aligned} AR_{tot}(t) &= AR_1(t) + AR_2(t) \\ BR_{tot}(t) &= BR_1(t) + BR_2(t). \end{aligned} \quad (13)$$

Because of difficulties with estimating the binding rate constants for the R_2 receptor, we investigate the dynamics at the R_2 state more closely. Thus, we write the equations in (3), which involve R_2 separately in greater detail so that the parameters are all explicitly apparent:

$$\begin{cases} \frac{dAR_2}{dt} = k_3 A \cdot R_{2,tot} - (k_3 A + k_4) AR_2 - k_3 A \cdot BR_2 \\ \frac{dBR_2}{dt} = k_7 B \cdot R_{2,tot} - k_7 B \cdot AR_2 - (k_7 B + k_8) BR_2 \end{cases} \quad (14)$$

Subsequently, we divide them by their respective on-rates: the one for AR_2 by k_3 and the one for BR_2 by k_7 . This yields a system with the concentrations of AR_2 and BR_2 and the affinities of A ($K_{A,2}$) and B ($K_{B,2}$) to R_2 on the right:

$$\begin{cases} \frac{1}{k_3} \frac{dAR_2}{dt} = A \cdot R_{2,tot} - (A + K_{A,2}) AR_2 - A \cdot BR_2 \\ \frac{1}{k_7} \frac{dBR_2}{dt} = B \cdot R_{2,tot} - B \cdot AR_2 - (B + K_{B,2}) BR_2 \end{cases} \quad (15)$$

In this manner, we have singled out the on-rates on the left-hand sides of the two equations, and the right-hand side is entirely composed of concentrations and affinities.

We now scale the time variable and define $\tau = k_3 \cdot t$ so that AR_2 varies on a temporal scale of order unity. In addition, we define the ratio of k_3 and k_7 as ε and introduce this time-variable into the system (Equation 15) to yield

$$\begin{cases} \frac{dAR_2}{d\tau} = A \cdot R_{2,tot} - (A + K_{A,2}) AR_2 - A \cdot BR_2 \\ \varepsilon \frac{dBR_2}{d\tau} = B \cdot R_{2,tot} - B \cdot AR_2 - (B + K_{B,2}) BR_2 \end{cases} \quad \varepsilon = \frac{k_3}{k_7}. \quad (16)$$

If the ratio ε is much lower than unity, it follows from Singular Perturbation Theory (Bender and Orszag, 1999) that the dynamics of BR_2 is much faster than that of AR_2 and that BR_2 very quickly reaches a quasi-static state:

$$BR_2 = \frac{B}{B + K_{B,2}} (R_{2,tot} - AR_2), \quad (17)$$

so that BR_2 moves in lockstep with $(R_{2,tot} - AR_2)$, and the binding of AR_2 and BR_2 is quickly synchronized.

Data analysis

All experimental data were analysed using Graphpad Prism 6.0 (Graphpad Software, Inc., San Diego, CA, USA). Association data were fitted using *two phase association* to obtain the observed association rates (k_{A,R_1} and k_{A,R_2}). k_{on} values (k_1 and k_3) of [3H]-NECA were obtained from k_{A,R_1} and k_{A,R_2} values using Equation 4, where k_2 and k_4 were obtained from independent dissociation experiments. Dissociation data were fitted and allowed the software to compare with the extra-sum-of-square F test between the equations *Dissociation: one-phase exponential decay* and *biphasic exponential decay* (threshold P value ≤ 0.01). Association and dissociation rate constants for unlabelled ligands were calculated by fitting the data in the two-state competition association model (entering the model into Graphpad Prism 6.0 is detailed in Supporting Information). The data and statistical analysis comply with the recommendations on experimental design and analysis in pharmacology (Curtis *et al.*, 2015).

Materials

[3H]-NECA (specific activity 29.4 Ci·mmol $^{-1}$) was purchased from Perkin Elmer (Groningen, The Netherlands). Unlabelled NECA and DPCPX were purchased from Sigma-Aldrich (Steinheim, Germany), and CPA was obtained from Abcam (Cambridge, UK). LUF5962 was synthesized in our laboratory (Chang *et al.*, 2006). Adenosine deaminase was purchased from Boehringer Mannheim (Mannheim, Germany). CHAPS was obtained from Carl Roth GmbH (Karlsruhe, Germany). CHO cells stably expressing the human A_1 receptor (CHO A_1R) were kindly provided by Dr. K-N Klotz (University of Würzburg, Germany). All other chemicals were of analytical grade and obtained from standard commercial sources.

Nomenclature of targets and ligands

Key protein targets and ligands in this article are hyperlinked to corresponding entries in <http://www.guidetopharmacology.org>, the common portal for data from the IUPHAR/BPS Guide to PHARMACOLOGY (Harding *et al.*, 2018), and are permanently archived in the Concise Guide to PHARMACOLOGY 2017/2018 (Alexander *et al.*, 2017a,b,c).

Results

Quantification of the affinity of unlabelled ligands

The binding affinity of two representative agonists (NECA and CPA) and two antagonists (DPCPX and LUF5962) was determined in competition binding assays. All compounds tested produced concentration-dependent inhibition of specific [³H]-NECA binding (Figure 1), and their pIC₅₀ values are shown in Table 1. The obtained pIC₅₀ values of the four compounds were used to set the concentrations of the unlabelled ligand in the two-state competition association assay.

Kinetic characterization of the agonistic radioligand

The binding kinetics of [³H]-NECA on the adenosine A₁ receptor was obtained from kinetic radioligand binding assays. It follows from Figure 2 that both the association and dissociation profiles of [³H]-NECA to and from the A₁ receptor were biphasic, consisting of a fast and a slow phase. The kinetics of [³H]-NECA binding was calculated using Equation 4. The values are detailed in Table 2.

Validation of the two-state model for kinetic characterization of an unlabelled ligand in the presence of an agonistic radioligand

The two-state model describes the binding of both a labelled and an unlabelled ligand, the former having apparent distinct binding kinetics at two receptor states (R₁ and R₂). With the predetermined association and dissociation rate

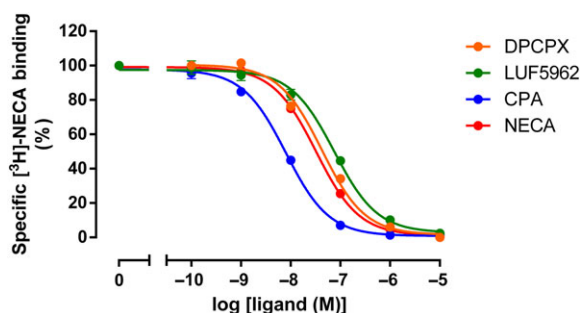


Figure 1

Displacement of [³H]-NECA by increasing concentrations of CPA, NECA, LUF5962 and DPCPX at the human adenosine A₁ receptor. Data shown are the mean ± SEM of five independent experiments, each performed in duplicate.

Table 1

Affinities (pIC₅₀ values) of CPA, NECA, LUF5962 and DPCPX for the human A₁ receptor

Compound	CPA	NECA	LUF5962	DPCPX
pIC ₅₀	8.10 ± 0.03	7.49 ± 0.03	7.13 ± 0.05	7.23 ± 0.05

Data are the mean ± SEM of five separate experiments each performed in duplicate.

constants of [³H]-NECA, it was possible to measure the binding kinetics of unlabelled ligands using the two-state model (Figure 3A). The unlabelled ligand was assayed at three different concentrations to ensure that (i) the ligand tested displayed competitive and reversible binding and (ii) the data were sufficiently dense for analysing with the two-state model. The data for unlabelled NECA are reported in Table 2. Its on-rate and off-rate constants (k₅ and k₆) at the R₁ state were similar to the values (k₁ and k₂) of [³H]-NECA. Likewise, the on-rate and off-rate constants (k₇ and k₈) of unlabelled NECA at the R₂ state were on the same order as those for [³H]-NECA (k₃ and k₄). This suggests that the model is suitable to determine the binding kinetics of unlabelled ligands.

Quantification of the association and dissociation rate constants of an unlabelled ligand

The binding kinetics of another representative A₁ receptor agonist (CPA) was examined subsequently. As shown in Table 3 and Figure 3B, rate constants for unlabelled CPA can be determined using the two-state model. Moreover, two representative A₁ receptor antagonists, LUF5962 and DPCPX, were characterized using the two-state model. As shown in Figure 3C, D, the model appears to fit the data well for both antagonists. This allowed us to determine the kinetics of the two compounds at the R₁ state (Table 3). However, k₇ and k₈ of these two antagonists at the R₂ state were ambiguous with very wide 95% confidence intervals. Evidently, the two-state model has limitations in determining the kinetics of some unlabelled ligands and, in particular, antagonists.

Data simulations

Data simulations were performed to further validate the two-state model for kinetic characterization of the binding kinetics of an unlabelled ligand and to explore the limitations of the model for kinetic measurements.

First, we simulated the system (Equation 3) for competitive binding of the radioligand [³H]-NECA in the presence of unlabelled NECA to the receptor. Kinetic parameters of both [³H]-NECA and NECA were obtained from experimental measurements. It follows from Figure 4A that the simulated data were similar to the experimental data, suggesting once more that the model is suited to determine the binding kinetics of unlabelled ligands. Furthermore, we only simulated the system (Equation 6) for the total binding of [³H]-NECA at steady state (AR_{tot} = AR_{1,ss} + AR_{2,ss}) in the presence of NECA or CPA at different concentrations, as the binding of [³H]-NECA in the presence of DPCPX or LUF5962 could not be simulated due to the ambiguous values for k₇ and k₈. This then allowed us to compare the simulated results with the

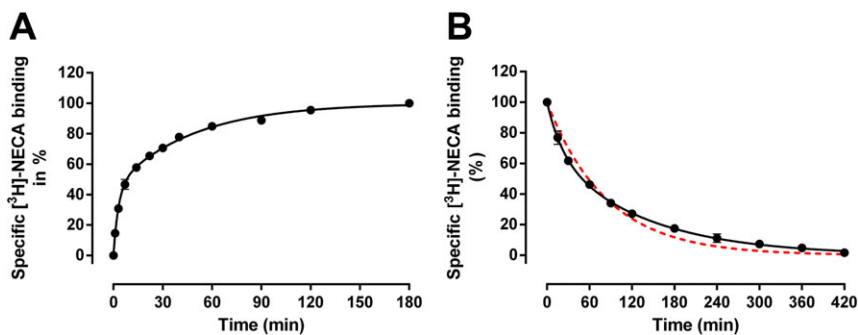


Figure 2

(A) The association of [³H]-NECA to the human adenosine A₁ receptor. Data shown are the mean ± SEM of seven independent experiments, each performed in duplicate (B). The dissociation of [³H]-NECA from the human adenosine A₁ receptor. Data are the mean ± SEM of five independent experiments, each performed in duplicate. Data were best fitted using a biphasic exponential decay (black solid line, comparison with the extra-sum-of-square F test, *P* value <0.0501). The rejected one phase exponential decay fitting of the data is shown with the red dotted line.

Table 2

Kinetic profiles of [³H]-NECA and unlabelled NECA on the human A₁ receptor

	k_1 (M ⁻¹ ·min ⁻¹)	k_2 (min ⁻¹)	$K_{A,1}$ (nM)	k_3 (M ⁻¹ ·min ⁻¹)	k_4 (min ⁻¹)	$K_{A,2}$ (nM) ^c	Fraction fast (%) ^c
[³ H]-NECA ^a	$1.4 \pm 0.2 \times 10^7$	0.046 ± 0.007	3.2 ± 0.7	$5.8 \pm 0.5 \times 10^5$	0.0076 ± 0.0004	13 ± 1	32 ± 4
	k_5 (M ⁻¹ ·min ⁻¹)	k_6 (min ⁻¹)	$K_{B,1}$ (nM)	k_7 (M ⁻¹ ·min ⁻¹)	k_8 (min ⁻¹)	$K_{B,2}$ (nM)	–
NECA ^b	$1.4 \pm 0.2 \times 10^7$	0.074 ± 0.019	5.3 ± 1.6	$1.1 \pm 0.6 \times 10^6$	0.019 ± 0.007	17 ± 11	–

^aData were obtained from kinetic radioligand binding experiments on the A₁ receptor. Data are the mean ± SEM of seven (association) and five (dissociation) separate experiments, respectively, each performed in duplicate. $K_{A,1} = k_2/k_1$ and $K_{A,2} = k_4/k_3$

^bData were obtained from two-state competition association assay on the A₁ receptor. Data are the mean ± SEM of five separate experiments each performed in duplicate. $K_{B,1} = k_6/k_5$ and $K_{B,2} = k_8/k_7$

^cData were obtained from radioligand dissociation experiments on the A₁ receptor and fitted in *two-phase exponential decay*. Data are the mean ± SEM of five separate experiments each performed in duplicate.

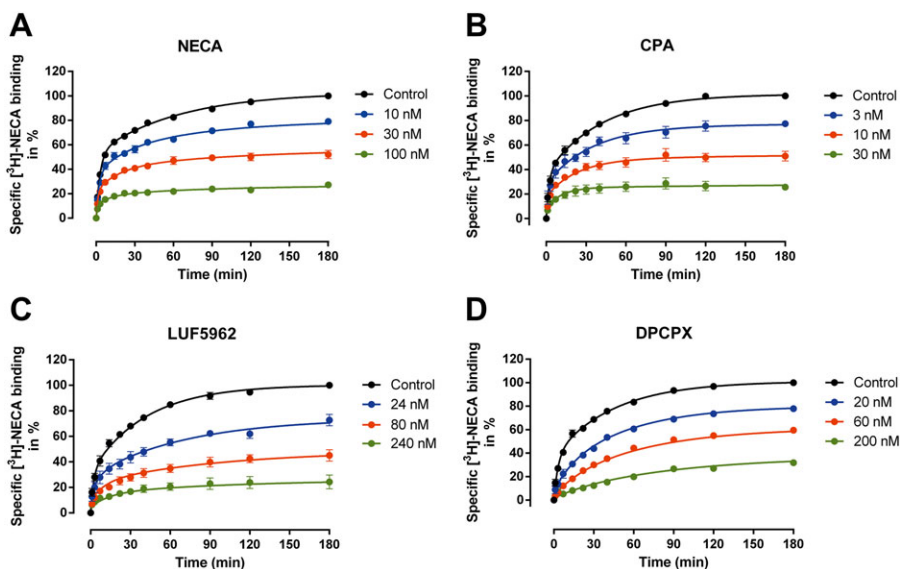


Figure 3

Two-state competition association experiment with [³H]-NECA in the absence or presence of unlabelled NECA (A), CPA (B), LUF5962 (C) and DPCPX (D). Data shown are the mean ± SEM of five independent experiments, each performed in duplicate.

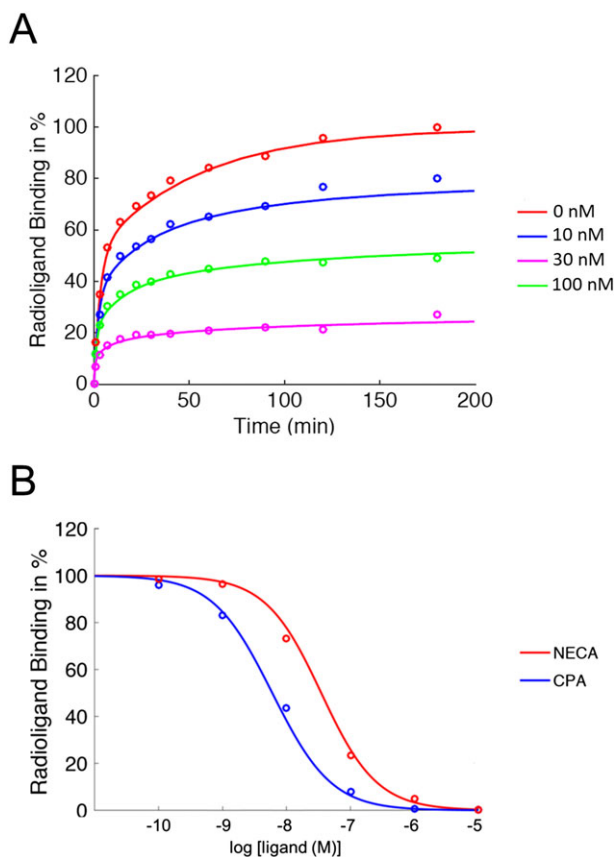
Table 3

Kinetic profiles of an unlabelled agonist, CPA and two unlabelled antagonists, DPCPX and LUF5962, on the human A₁ receptor using the two-state model

	k_5 ($M^{-1} \cdot \text{min}^{-1}$)	k_6 (min^{-1})	$K_{B,1}$ (nM)	k_7 ($M^{-1} \cdot \text{min}^{-1}$)	k_8 (min^{-1})	$K_{B,2}$ (nM)
CPA	$5.2 \pm 0.1 \times 10^7$	0.025 ± 0.011	0.48 ± 0.21	$1.8 \pm 0.4 \times 10^6$	0.0095 ± 0.0032	5.2 ± 2.1
DPCPX	$2.1 \pm 1.4 \times 10^8$	0.78 ± 1.42	3.7 ± 7.1	6.2×10^{13a}	3.4×10^{6a}	55^a
LUF5962	$1.0 \pm 0.4 \times 10^7$	0.23 ± 0.10	23 ± 66	2.3×10^{14a}	3.4×10^{6a}	15^a

Data are the mean \pm SEM of five separate experiments each performed in duplicate. Data were obtained from two-state competition association assay on the A₁R.

^aMean values obtained by using the two-state model. Data were ambiguous with very wide 95% confidence intervals.

**Figure 4**

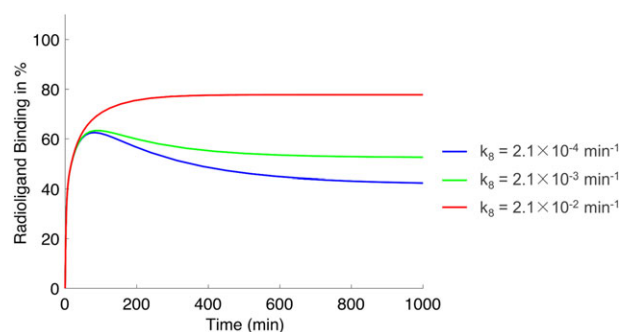
(A) Comparison of the simulated kinetic radioligand binding (lines) with the experimental data (circles) of [³H]-NECA in the presence of unlabelled NECA at different concentrations (0 nM; 10 nM; 30 nM and 100 nM). Data are shown as normalized values to the total binding of the radioligand at both R₁ and R₂ states. (B) Comparison of the simulated radioligand binding (lines) at the steady state with the experimental data from [³H]-NECA displacement experiments in the presence of a competitor at different concentrations (1×10^{-10} M to 1×10^{-5} M; circles). The kinetic parameters of [³H]-NECA and the competitors (NECA and CPA) for data simulations were obtained from Tables 2 and 3. Data are shown as normalized values to the total binding of the radioligand at both R₁ and R₂ states.

experimental data from the competition binding assays (Figure 1). As shown in Figure 4B, the simulated data were in accordance with our experimental determinations, further

confirming that the model is sufficient to determine the binding kinetics of unlabelled ligands. In addition, we performed data simulations using different k_8 values while maintaining other parameters identical (Figure 5). We found that a slow dissociation from one receptor state can induce an 'overshoot' (as in the blue and green curves), and the pattern becomes more significant with a significantly smaller k_8 value. As shown in Figure 5, a compound with a k_8 value of $2.1 \times 10^{-4} \text{ min}^{-1}$ displayed a clear overshoot while the compound with a 100-fold larger k_8 value ($2.1 \times 10^{-2} \text{ min}^{-1}$) did not.

Investigating the limitations of the current radioligand in determining the binding kinetics with the two-state model

The two-state model can reproduce and quantify the binding kinetics of NECA and CPA, as demonstrated by both experimental and simulation results. However, k_7 and k_8 values for DPCPX and LUF5962 could not be accurately determined in the two-state model by using [³H]-NECA, which displayed relatively slow kinetics at both R₁ ($k_1 = 1.4 \pm 0.2 \times 10^7 \text{ M}^{-1} \cdot \text{min}^{-1}$, $k_2 = 0.046 \pm 0.007 \text{ min}^{-1}$) and R₂ states ($k_3 = 5.8 \pm 0.5 \times 10^5 \text{ M}^{-1} \cdot \text{min}^{-1}$ and $k_4 = 0.0076 \pm 0.0004 \text{ min}^{-1}$). Additional data analysis was therefore performed to understand the limitations of using

**Figure 5**

Data simulations of [³H]-NECA in the presence of ligands with different k_8 values ($2.1 \times 10^{-2} \text{ min}^{-1}$; $2.1 \times 10^{-3} \text{ min}^{-1}$; $2.1 \times 10^{-4} \text{ min}^{-1}$) while k_5 ($1.4 \times 10^7 \text{ M}^{-1} \cdot \text{min}^{-1}$), k_6 (0.074 min^{-1}) and k_7 ($1.1 \times 10^6 \text{ M}^{-1} \cdot \text{min}^{-1}$) were kept constant. The kinetic parameters of [³H]-NECA for data simulations were obtained from Table 2. Data are shown as normalized values to the total binding of the radioligand at both R₁ and R₂ states.

the current radioligand. Given that the kinetics for both compounds was ambiguous at the R_2 state, we specifically focused on the binding of the radioligand and the competitor in the system (Equation 14). Upon simulating the binding of BR_2 with different ϵ values ($\epsilon = k_3/k_7$, Figure 6), we observed that the time for BR_2 to reach the quasi-static state (Equation 17) was indeed shorter after changing the k_7 values, while keeping the K_{B,R_2} fixed at 55 nM. Notably, when ϵ was small (Figure 6A, $\epsilon = 1.5 \times 10^{-8}$; and Figure 6B, $\epsilon = 1.5 \times 10^{-3}$), BR_2 reached the quasi-static state in much less than 1 min, which was, in fact, our first experimental assay point. This implies that the transient binding of A and B at the R_2 state cannot be sufficiently recorded experimentally before the quasi-static state has been reached. As a result, kinetic characterization of an unlabelled ligand at the R_2 state becomes unreliable, which is probably the case for the antagonists DPCPX and LUF5962. Indeed, the association rates of DPCPX and LUF5962 were $2.0 \times 10^8 \text{ M}^{-1} \cdot \text{min}^{-1}$ and $1.2 \times 10^8 \text{ M}^{-1} \cdot \text{min}^{-1}$, respectively, determined previously at 25°C (Guo *et al.*, 2013), and it is therefore reasonable to speculate that the values will be even higher at 30°C, hence resulting in ϵ values lower than 0.001. In contrast, when ϵ was increased to 0.15 or 1.5, the binding of BR_2 required a longer incubation period (i.e. more than

3 min) to reach the quasi-static state (Figure 6C, D). Notably, the ϵ values for NECA and CPA were determined as 0.52 ($k_3/k_7 = 5.8 \times 10^5/1.1 \times 10^6$, data from Table 2) and 0.32 ($k_3/k_7 = 5.8 \times 10^5/1.8 \times 10^6$, data from Tables 2 and 3), respectively, that is, significantly higher than the ϵ values of DPCPX and LUF5962, hence resulting in reliable kinetic measurements.

Furthermore, we compared the simulated competitive association of the radioligand [^3H]-NECA to the receptor in the presence of unlabelled DPCPX with the experimental data (Figure 7). It follows from Figure 7A that the simulated data were similar to the experimental data. Next, we reduced the k_7 value of DPCPX to $6.2 \times 10^8 \text{ M}^{-1} \cdot \text{min}^{-1}$ (Figure 7B), $6.2 \times 10^6 \text{ M}^{-1} \cdot \text{min}^{-1}$ (Figure 7C) and $6.2 \times 10^5 \text{ M}^{-1} \cdot \text{min}^{-1}$ (Figure 7D). This yielded corresponding ϵ values of 1.5×10^{-3} , 0.15 and 1.5. Simultaneously, the k_8 values were reduced to 3.4 min^{-1} , 0.034 min^{-1} and 0.0034 min^{-1} , respectively, so that $K_{B,2}$ was kept fixed at 55 nM. Interestingly, the simulated curves in Figure 7B, C for the reduced rate constants fit the experimental data just as well as those in Figure 7A. In contrast, when further increasing the ϵ value to 1.5 (Figure 7D), the simulated curves significantly deviated from the experimental data. Together, these results

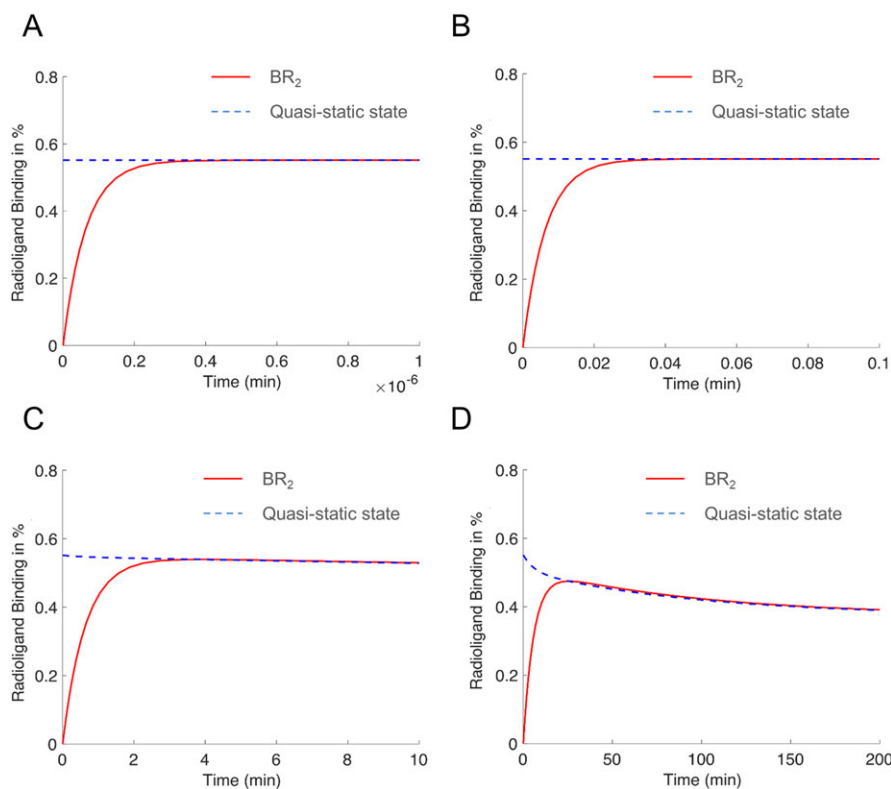


Figure 6

Data simulations of the binding of DPCPX (200 nM) at the R_2 state (BR_2) and its binding at the quasi-static state. The off-rates of [^3H]-NECA from the R_1 and R_2 states for simulations were from radioligand dissociation experiments ($k_2 = 0.046 \text{ min}^{-1}$ and $k_4 = 0.0076 \text{ min}^{-1}$), while the on-rates of [^3H]-NECA to the R_1 and R_2 states for simulation were obtained by analysing the kinetic binding of [^3H]-NECA in the absence of the competitor in the two-state competition association assays ($k_1 = 1.4 \times 10^7 \text{ M}^{-1} \cdot \text{min}^{-1}$, $k_3 = 1.1 \times 10^6 \text{ M}^{-1} \cdot \text{min}^{-1}$). The k_5 and k_6 values of unlabelled DPCPX for simulation were $2.1 \times 10^8 \text{ M}^{-1} \cdot \text{min}^{-1}$ and 0.775 min^{-1} respectively. The k_7 and k_8 values of unlabelled DPCPX for simulation were (A) $6.2 \times 10^{13} \text{ M}^{-1} \cdot \text{min}^{-1}$ and $3.4 \times 10^5 \text{ min}^{-1}$, (B) $6.2 \times 10^8 \text{ M}^{-1} \cdot \text{min}^{-1}$ and 3.4 min^{-1} , (C) $6.2 \times 10^6 \text{ M}^{-1} \cdot \text{min}^{-1}$ and 0.034 min^{-1} or (D) $6.2 \times 10^5 \text{ M}^{-1} \cdot \text{min}^{-1}$ and 0.0034 min^{-1} .

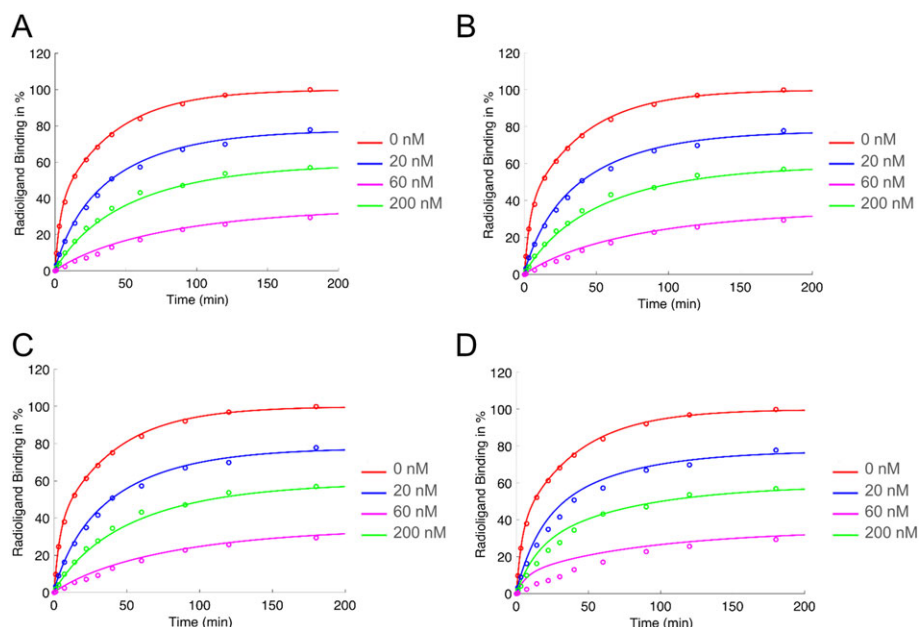


Figure 7

Comparison of the simulated kinetic radioligand binding (lines) with the experimental data (circles) of [³H]-NECA in the presence of unlabelled DPCPX at different concentrations (0 nM; 20 nM; 60 nM and 200 nM). Data are shown as normalized values to the total binding of the radioligand at both R₁ and R₂ states. The off-rates of [³H]-NECA from the R₁ and R₂ states for simulation were from radioligand dissociation experiments ($k_2 = 0.046 \text{ min}^{-1}$ and $k_4 = 0.0076 \text{ min}^{-1}$), while the on-rates of [³H]-NECA to the R₁ and R₂ states for simulation were obtained by analysing the kinetic binding of [³H]-NECA in the absence of the competitor in the two-state competition association assays ($k_1 = 1.4 \times 10^7 \text{ M}^{-1} \cdot \text{min}^{-1}$, $k_3 = 1.1 \times 10^6 \text{ M}^{-1} \cdot \text{min}^{-1}$). The k_5 and k_6 values of unlabelled DPCPX for simulation were $2.1 \times 10^8 \text{ M}^{-1} \cdot \text{min}^{-1}$ and 0.775 min^{-1} respectively. The k_7 and k_8 values of unlabelled DPCPX for simulation were (A) $6.2 \times 10^{13} \text{ M}^{-1} \cdot \text{min}^{-1}$ and $3.4 \times 10^5 \text{ min}^{-1}$, (B) $6.2 \times 10^8 \text{ M}^{-1} \cdot \text{min}^{-1}$ and 3.4 min^{-1} , (C) $6.2 \times 10^6 \text{ M}^{-1} \cdot \text{min}^{-1}$ and 0.034 min^{-1} or (D) $6.2 \times 10^5 \text{ M}^{-1} \cdot \text{min}^{-1}$ and 0.0034 min^{-1} .

imply that the kinetics of DPCPX at the R₂ state was very fast with a low ϵ value (at least less than 1.5). In our current work, the actual magnitude of k_7 and k_8 of an antagonist has little effect on the graph of AR₂(t), reflecting the ambiguous k_7 and k_8 values for DPCPX determined by the two-state model.

Discussion

The Motulsky and Mahan model makes it possible to measure the binding kinetics of an unlabelled ligand, which provides the practical convenience of not needing to label every ligand of interest (Motulsky and Mahan, 1984). However, the application of the model is limited because of the assumption that the labelled reference ligand does not have preference for any particular receptor state, hence representing a one-state model. A labelled probe, for example, a radioligand, may display biphasic kinetic binding, representing different binding kinetics to different receptor states (Munshi *et al.*, 1985; van Veldhoven *et al.*, 2015). A number of reasons may be relevant to the nature of the biphasic kinetic binding. For a GPCR as an example, there may be an active state bound to a G protein and an inactive state that is not bound to a G protein. It is also possible that the kinetic difference is due to the ligand interacting with receptors that exist in various structures of membrane preparations. For instance, a portion of the receptors may be present in vesicular structures, and are thus less

accessible (Cohen *et al.*, 1996). Similarly, for other drug targets, different states or conformations may exist, for instance, an ion channel has open and closed states (Hill *et al.*, 2014). Whatever the reason, under these circumstances the kinetics of unlabelled ligand binding cannot be characterized. Thus, it is important to develop a new mathematical model for a two-state system, yielding a quantitative assessment of the kinetic parameters of both probe and unlabelled competitor. In the present study, we have developed and validated such a two-state model for kinetic characterization. This method may well fill a niche and become of practical value, especially for targets for which a radiolabelled antagonist is not available, such as the **HCA receptors** (Offermanns *et al.*, 2011), or targets where the radiolabelled antagonist is not ideal for accurate kinetic measurements due to high non-specific binding.

An important variable to optimize in the two-state model for accurate kinetic determinations was the concentration of the unlabelled ligand as in the one-state model (Dowling and Charlton, 2006). Firstly, it appeared necessary to use at least three concentrations to ensure reliable calculations. Reducing assay points with fewer concentrations tends to compromise the quality of the data analysis with lower reliability or even ambiguity, as reflected by wider 95% confidence intervals. Secondly, we found that lower competitor concentrations will have little influence on the radioligand association process, leading to a high degree of error in rate estimates for the unlabelled ligand. In contrast, a higher concentration of the competing ligand might cause little

radioligand binding remaining, also preventing a meaningful data analysis. Thus, we used 0.3-fold, 1-fold and 3-fold of the IC_{50} value of the relevant compound, obtained from displacement experiments to generate reproducible and accurate rate constants.

We also found other assay conditions that are critical for accurate kinetic determinations. It is essential to include sufficient time points for the binding of the radioligand in the absence or presence of an unlabelled competitor, particularly in the fast associating phase and the intersection of both fast and slow phases (e.g. Figure 2, before 30 min), to better capture the biphasic association pattern of the agonistic radioligand. Another critical factor to optimize is the assay temperature. Increasing the assay temperature enhances the rates of association to both states. As a result, it might shift the biphasic radioligand association into a pseudo-one phasic process (which might also happen when one has sparse time points), hence affecting the accuracy of the assay. In the present study, we performed the assay at 30°C. At this temperature, the kinetics of [3H]-NECA at the R_1 state were $1.4 \pm 0.2 \times 10^7 M^{-1} \cdot \text{min}^{-1}$ (association) and $0.046 \pm 0.007 \text{ min}^{-1}$ (dissociation). Thus, its observed association rate (k_{A,R_1}) can be calculated as 0.298 min^{-1} ($k_{A,R_1} = k_1 \times A + k_2$, $A = 18 \text{ nM}$). Similarly, its observed association rate (k_{A,R_2}) to the R_2 state can be calculated as 0.0178 min^{-1} ($k_{A,R_2} = k_3 \times A + k_4$, $k_3 = 5.8 \pm 0.5 \times 10^5 M^{-1} \cdot \text{min}^{-1}$, $k_4 = 0.0076 \pm 0.0004 \text{ min}^{-1}$, $A = 18 \text{ nM}$). Their respective half-lives are 2.33 min and 38.9 min ($t_{1/2,R_1} = \ln 2/k_{A,R_1}$, $t_{1/2,R_2} = \ln 2/k_{A,R_2}$), different by a factor of 17. Evidently, this difference is sufficient to generate the biphasic association curve of the radioligand. Furthermore, a critical condition for the successful application of the two-state model was found to be that the on-rate to each receptor, that is, k_1 and k_5 (R_1) as well as k_3 and k_7 (R_2) are of similar order of magnitude. This ensures that the resulting graphs are truly biphasic and clearly exhibit the different convergence rates involved.

According to the theory for a one-state model developed by Motulsky and Mahan, initial radioligand binding overshoots its equilibrium occupancy when the dissociation of the competitor is slower than that of the radioligand. An example was provided in our previous research, in which an **A_{2A} receptor** agonist, **UK432,097**, displayed a slower dissociation rate constant ($k_{\text{off}} = 0.004 \text{ min}^{-1}$) than the radioligand ($k_{\text{off}} = 0.01 \text{ min}^{-1}$), resulting in an initial overshoot of radioligand binding (Guo *et al.*, 2012). The theoretical basis of this overshoot also allows one to modify the full competition association assay into a high-throughput format, enabling fast kinetic screening (Guo *et al.*, 2013). In comparison, the two-state system contains two sets of 'micro-kinetics', which increases the difficulty of qualitatively judging the occurrence of overshoot. An overshoot will occur if $k_6 < k_2$ and $k_8 < k_4$; and an overshoot will not occur if $k_6 > k_2$ and $k_8 > k_4$. In cases where $k_6 < k_2$ and $k_8 > k_4$ or $k_6 > k_2$ and $k_8 < k_4$, the overshoot may or may not occur, depending on the relative ratio of the R_1 and R_2 populations, as well as the values of the rate constants k_6 and k_8 . In the present study, CPA displayed faster dissociation rate constants compared with the radioligand, and no overshoot was observed indeed. We also performed data simulations using different k_8 values while maintaining other parameters identical. It follows from Figure 5 that a slow dissociation from

one receptor state can induce the overshoot, and the pattern becomes more significant with a significantly smaller k_8 value (i.e. $k_8 = 0.0021 \text{ min}^{-1}$) while not so for the case where k_8 is 10-fold faster. Thus, one needs to be cautious in using the overshoot phenomenon for kinetic screening in the context of a two-state model.

The two-state model enables us to separate the binding kinetics to two receptor states. However, one needs to consider several limitations while applying the model for kinetic measurements. Firstly, one cannot attribute the values at the R_1 and R_2 states to a specific conformation or state of the receptor. For GPCRs, it is likely that the fast association/dissociation phase is related to the G protein-uncoupled state/the inactive state, while the slow association/dissociation phase is correlated to the G protein-coupled state/the active state (Casarosa *et al.*, 2011; Cohen *et al.*, 1996). Secondly, it is also important to point out that the kinetic characterization was performed using membrane preparations, where we assume both R_1 and R_2 populations are unable to significantly convert into each other, at least during the time frame of the measurements. However, under other conditions, such as in whole-cell based experiments, both populations are not necessarily fixed (Kenakin, 2001), and their respective magnitude is able to vary in the often-evoked induced-fit model (Vauquelin *et al.*, 2016), not only for agonists (De Lean *et al.*, 1980) but also for antagonists (Vauquelin *et al.*, 2001). In these circumstances, one should be cautious in using the two-state model for kinetic determinations. Instead, numerical simulations might be needed for such more complex situations (Woodroffe *et al.*, 2009; Bridge *et al.*, 2010). Thirdly, if the radioligand has relatively slow association kinetics, it might yield limitations in measuring unlabelled ligands with faster kinetics, as seems to be the case for DPCPX and LUF5962. One could consider using another radioligand with faster association kinetics, if available, to increase the ratio of k_3 and k_7 . Additionally, the method remains laborious as it requires a sufficiently high number of data points for reliable kinetic estimation. To further adapt the assay into a high-throughput format, one may consider combining the two-state model with homogenous binding assay techniques, such as the scintillation proximity assay (Xia *et al.*, 2016) or the time-resolved fluorescence energy transfer assay (Schiele *et al.*, 2015; Nederpelt *et al.*, 2016), which allow continuous readout of ligand-receptor binding without physical separation between free and bound ligands.

To conclude, we have introduced a two-state model containing two receptor states, R_1 and R_2 , for kinetic profiling of an unlabelled competitor using an agonist radioligand. The new model comprises a linear system of ODEs for which we can find analytical solutions. This makes further analysis feasible and is straightforward to simulate with (no need for numerical differential equation solvers). We believe that with the correct technical application of the two-state model, one can determine the kinetics of unlabelled ligands using an agonist radioligand, as shown for ligands at the human adenosine A_1 receptor, as a prototypical GPCR. The two-state model may have general applicability on other drug targets as well, thereby enabling more kinetics-directed research in the early phases of the drug discovery process.

Acknowledgements

This research received support from the Innovative Medicines Initiative Joint Undertaking under K4DD (www.k4dd.eu), grant agreement no. 115366, resources of which are composed of financial contribution from the European Union's Seventh Framework Programme (FP7/2007-2013) and European Federation of Pharmaceutical Industries and Associations (EFPIA) companies' in-kind contribution. This research received support from National Natural Science Foundation of China (no. 81603170 to D.G.) and Natural Science Foundation of Jiangsu Province (no. BK20160234 to D.G.).

Author contributions

D.G., L.A.P., A.Z., L.H.H. and A.P.I.J. participated in the making of research design. D.G., L.A.P., L.B., W.K. and H.D.V. conducted the experiments. D.G., L.A.P., L.B., W.K., A.Z., L.H.H. and A.P.I.J. performed the analysis of data. D.G., L.A.P., L.B., L.H.H. and A.P.I.J. wrote or contributed to the writing of the manuscript.

Conflicts of interest

The authors declare no conflicts of interest.

Declaration of transparency and scientific rigour

This Declaration acknowledges that this paper adheres to the principles for transparent reporting and scientific rigour of preclinical research recommended by funding agencies, publishers and other organisations engaged with supporting research.

References

- Alexander SPH, Christopoulos A, Davenport AP, Kelly E, Marrion NV, Peters JA *et al.* (2017a). The Concise Guide to PHARMACOLOGY 2017/18: G protein-coupled receptors. *Br J Pharmacol* 174 (Suppl 1): S17–S129.
- Alexander SPH, Striessnig J, Kelly E, Marrion NV, Peters JA, Faccenda E *et al.* (2017b). The Concise Guide to PHARMACOLOGY 2017/18: Voltage-gated ion channels. *Br J Pharmacol* 174: S160–S194.
- Alexander SPH, Fabbro D, Kelly E, Marrion NV, Peters JA, Faccenda E *et al.* (2017c). The Concise Guide to PHARMACOLOGY 2017/18: Enzymes. *Br J Pharmacol* 174: S272–S359.
- Bridge LJ, King JR, Hill SJ, Owen MR (2010). Mathematical modelling of signalling in a two-ligand G-protein coupled receptor system: agonist-antagonist competition. *Math Biosci* 223: 115–132.
- Bender CM, Orszag AO (1999). *Advanced Mathematical Methods For Scientists And Engineers*. Springer-Verlag: New York.
- Casarosa P, Kollak I, Kiechle T, Ostermann A, Schnapp A, Kiesling R *et al.* (2011). Functional and biochemical rationales for the 24-hour long duration of action of olodaterol. *J Pharmacol Exp Ther* 337: 600–609.
- Chang LC, Spanjersberg RF, Von Frijtag Drabbe Kunzel JK, Mulder-Krieger T, Brussee J *et al.* (2006). 2,6-disubstituted and 2,6,8-trisubstituted purines as adenosine receptor antagonists. *J Med Chem* 49: 2861–2867.
- Cohen FR, Lazareno S, Birdsall NJ (1996). The effects of saponin on the binding and functional properties of the human adenosine A₁ receptor. *Br J Pharmacol* 117: 1521–1529.
- Copeland RA (2016). The drug-target residence time model: a 10-year retrospective. *Nat Rev Drug Discov* 15: 87–95.
- Copeland RA, Pompliano DL, Meek TD (2006). Drug-target residence time and its implications for lead optimization. *Nat Rev Drug Discov* 5: 730–739.
- Curtis MJ, Bond RA, Spina D, Ahluwalia A, Alexander SPA, Giembycz MA *et al.* (2015). Experimental design and analysis and their reporting: new guidance for publication in *BJP*. *Br J Pharmacol* 172: 3461–3471.
- De Lean A, Stadel JM, Lefkowitz RJ (1980). A ternary complex model explains the agonist-specific binding properties of the adenylate cyclase-coupled beta-adrenergic receptor. *J Biol Chem* 255: 7108–7117.
- Dowling MR, Charlton SJ (2006). Quantifying the association and dissociation rates of unlabelled antagonists at the muscarinic M₃ receptor. *Br J Pharmacol* 148: 927–937.
- Guo D, Heitman LH, IJzerman AP (2017). Kinetic aspects of the interaction between ligand and G protein-coupled receptor: the case of the adenosine receptors. *Chem Rev* 117: 38–66.
- Guo D, Hillger JM, IJzerman AP, Heitman LH (2014). Drug-target residence time—a case for G protein-coupled receptors. *Med Res Rev* 34: 856–892.
- Guo D, Mulder-Krieger T, IJzerman AP, Heitman LH (2012). Functional efficacy of adenosine A_{2A} receptor agonists is positively correlated to their receptor residence time. *Br J Pharmacol* 166: 1846–1859.
- Guo D, Van Dorp EJ, Mulder-Krieger T, Van Veldhoven JP, Brussee J, IJzerman AP *et al.* (2013). Dual-point competition association assay: a fast and high-throughput kinetic screening method for assessing ligand-receptor binding kinetics. *J Biomol Screen* 18: 309–320.
- Harding SD, Sharman JL, Faccenda E, Southan C, Pawson AJ, Ireland S *et al.* (2018). The IUPHAR/BPS Guide to PHARMACOLOGY in 2018: updates and expansion to encompass the new guide to IMMUNOPHARMACOLOGY. *Nucl Acids Res* 46: D1091–D1106.
- Hill AP, Perrin MJ, Heide J, Campbell TJ, Mann SA, Vandenberg JI (2014). Kinetics of drug interaction with the Kv11.1 potassium channel. *Mol Pharmacol* 85: 769–776.
- Hoffmann C, Castro M, Rinken A, Leurs R, Hill SJ, Vischer HF (2015). Ligand residence time at G-protein-coupled receptors – why we should take our time to study it. *Mol Pharmacol* 88: 552–560.
- Kenakin T (2001). Inverse, protean, and ligand-selective agonism: matters of receptor conformation. *FASEB J* 15: 598–611.
- Malany S, Hernandez LM, Smith WF, Crowe PD, Hoare SR (2009). Analytical method for simultaneously measuring ex vivo drug receptor occupancy and dissociation rate: application to (R)-dimethindene occupancy of central histamine H₁ receptors. *J Recept Signal Transduct Res* 29: 84–93.

- Motulsky HJ, Mahan LC (1984). The kinetics of competitive radioligand binding predicted by the law of mass action. *Mol Pharmacol* 25: 1–9.
- Munshi R, Hansske F, Baer HP (1985). [125 I]N⁶-(3-iodo-4-hydroxyphenyl)isopropyladenosine: the use of the diastereomers as ligands for adenosine receptors in rat brain. *Eur J Pharmacol* 111: 107–115.
- Nederpelt I, Georgi V, Schiele F, Nowak-Reppel K, Fernandez-Montalvan AE, IJzerman AP *et al.* (2016). Characterization of 12 GnRH peptide agonists – a kinetic perspective. *Br J Pharmacol* 173: 128–141.
- Offermanns S, Colletti SL, Lovenberg TW, Semple G, Wise A, IJzerman AP (2011). International Union of Basic and Clinical Pharmacology. LXXXII: nomenclature and classification of hydroxy-carboxylic acid receptors (GPR81, GPR109A, and GPR109B). *Pharmacol Rev* 63: 269–290.
- Packeu A, Wennerberg M, Balendran A, Vauquelin G (2010). Estimation of the dissociation rate of unlabelled ligand-receptor complexes by a 'two-step' competition binding approach. *Br J Pharmacol* 161: 1311–1328.
- Schiele F, Ayaz P, Fernandez-Montalvan A (2015). A universal homogeneous assay for high-throughput determination of binding kinetics. *Anal Biochem* 468: 42–49.
- Smith PK, Krohn RI, Hermanson GT, Mallia AK, Gartner FH, Provenzano MD *et al.* (1985). Measurement of protein using bicinchoninic acid. *Anal Biochem* 150: 76–85.
- Swinney DC (2009). The role of binding kinetics in therapeutically useful drug action. *Curr Opin Drug Discov Devel* 12: 31–39.
- Swinney DC, Haubrich BA, Liefde IV, Vauquelin G (2015). The role of binding kinetics in GPCR drug discovery. *Curr Top Med Chem* 15: 2504–2522.
- Van Veldhoven JP, Liu R, Thee SA, Wouters Y, Verhoorck SJ, Mooiman C *et al.* (2015). Affinity and kinetics study of anthranilic acids as HCA2 receptor agonists. *Bioorg Med Chem* 23: 4013–4025.
- Vauquelin G, Fierensilse F, Vanderheyden V (2001). Insurmountable AT₁ receptor antagonism: fitting models with experimental data. *Trends Pharmacol Sci* 22: 557.
- Vauquelin G, Van Liefde I, Swinney DC (2016). On the different experimental manifestations of two-state 'induced-fit' binding of drugs to their cellular targets. *Br J Pharmacol* 173: 1268–1285.
- Vilums M, Zweemer AJ, Yu Z, De Vries H, Hillger JM, Wapenaar H *et al.* (2013). Structure–kinetic relationships – an overlooked parameter in hit-to-lead optimization: a case of cyclopentylamines as chemokine receptor 2 antagonists. *J Med Chem* 56: 7706–7714.
- Woodroffe PJ, Bridge LJ, King JR, Hill SJ (2009). Modelling the activation of G-protein coupled receptors by a single drug. *Math Biosci* 219: 32–55.
- Xia L, De Vries H, IJzerman AP, Heitman LH (2016). Scintillation proximity assay (SPA) as a new approach to determine a ligand's kinetic profile. A case in point for the adenosine A₁ receptor. *Purinergic Signal* 12: 115–126.
- Yu Z, IJzerman AP, Heitman LH (2015). Kv11.1 (hERG)-induced cardiotoxicity: a molecular insight from a binding kinetics study of prototypical Kv11.1 (hERG) inhibitors. *Br J Pharmacol* 172: 940–955.

Supporting Information

Additional Supporting Information may be found online in the supporting information tab for this article.

<https://doi.org/10.1111/bph.14184>

Data S1 Entering the two-state model for the kinetics of competitive radioligand binding into Graphpad Prism 6.0.